SI-Appendix

The CC domain structure from the wheat stem rust resistance protein Sr33 challenges paradigms for dimerization in plant NLR proteins

Lachlan W. Casey[a,1], Peter Lavrencic[a,b,1], Adam Bentham[a,c,1], Stella Cesari[d], Daniel J. Ericsson[e], Tristan I. Croll[f], Dusan Turk[g], Peter A. Anderson[c], Alan E. Mark[a], Peter N. Dodds[d], Mehdi Mobli[b,2], Bostjan Kobe[a,2] and Simon J. Williams[a,c,h,2]

[a]School of Chemistry and Molecular Biosciences, Institute for Molecular Bioscience and Australian Infectious Diseases Research Centre, University of Queensland, Brisbane, Queensland 4072, Australia. [b]Centre for Advanced Imaging, University of Queensland, Brisbane, Queensland 4072, Australia. [c]School of Biological Sciences, Flinders University, Adelaide, SA 5001, Australia. [d]CSIRO Agriculture, Canberra ACT 2601, Australia. [e]Macromolecular Crystallography Beamlines, Australian Synchrotron, Melbourne, Victoria 3168, Australia. [f]School of Biomedical Sciences, Queensland University of Technology, Brisbane, Queensland 4001, Australia. [g]Centre of Excellence for Integrated Approaches in Chemistry and Biology of Proteins; International Postgraduate School Jozef Stefan; Jozef Stefan Institute, 1000 Ljubljana, Slovenia. [h]Plant Sciences Division, Research School of Biology, The Australian National University, Canberra 2601, Australia.

[1]These authors contributed equally to this work

[2]To whom correspondence may be addressed**.** Email: s.williams8@uq.edu.au, b.kobe@uq.edu.au, or m.mobli@uq.edu.au.

SI Methods

Cloning, expression and purification.

The cDNAs coding for the proteins under study were cloned into the pMCSG7 vector by ligation-independent cloning (LIC). Primers designed for LIC consisted of gene-specific sequence, flanked by LIC overhangs to facilitate cloning into expression vectors. Details of primers and constructs used in cloning and expression are given in Tables S6 and S7. For Rx^{1-122}, a gBlock® of the codon optimised (*E. coli* expression) CC fragment with LIC sites was ordered from Integrated DNA Technologies (IDT) and cloned into expression vector pMCSG7.

For biophysical studies, the proteins were expressed in *Escherichia coli* BL21 (DE3) at 20˚C, using the autoinduction expression. Cells were lysed via sonication in the lysis buffer (consisting of 50 mM HEPES pH 8.0, 300 mM NaCl, and 1 mM dithiothreitol [DTT]) for $Sr33^{6-120}$, $MLA10^{5-120}$ and Rx^{1-122}. A similar lysis buffer was used for the longer CC domain fragments (corresponding to $Sr33^{6-144}$, $Sr33^{6-160}$, $MLA10^{5-144}$ and $MLA10^{5-160}$); however, the pH was adjusted to 7.5 and 500 mM of NaCl was used. The proteins were separated from clarified cell lysate via immobilized metal affinity chromatography (IMAC), facilitated by N-terminal 6 x histidine tags. Proteins were eluted from the IMAC column using elution buffer (consisting of 50 mM HEPES pH 7.5 and 8 [protein-dependent], 250 mM NaCl, and 250 mM imidazole). Post elution, excess imidazole was removed via buffer exchange, and proteins were maintained in a buffer consisting of 50 mM Tris-HCl pH 8.0, 250 mM NaCl and 1 mM DTT. Overnight treatment with TEV (tobacco etch virus) protease at 20˚C was used to remove the histidine tag, leaving a three-residue N-terminal overhang (Ser-Asp-Ala). SDS-PAGE analysis of proteins was used to follow the purification and removal of the histidine tag. The cleaved protein was re-applied to the nickel affinity chromatography column to remove the histidine tagged TEV protease and other contaminants. The proteins were further purified using a Superdex 75 HiLoad 26/60 size-exclusion chromatography (SEC) column (GE Healthcare) equilibrated with 10 mM HEPES pH 8.0, 150 mM NaCl and 1 mM DTT. Amicon® Ultra centrifugal filters (15 mL) (Merck Millipore) were used to concentrate proteins to appropriate concentrations for biophysical analysis, post-SEC.

We experienced considerable difficulties with expression and purification of $Sr50^{6-123}$. After much effort and optimisation we were able to obtain quantities of $Sr50^{6-123}$ that facilitated SEC-MALS analysis. This was achieved when using lysis, wash and elution buffers consisting of 1 M NaCl and 50 mM HEPES pH 8.5. Despite this, we still observed

significant protein loss during chromatography and concentration steps. These issues precluded Sr50$^{6-153}$ from further analysis using SEC-SAXS and structural studies.

Protein expression for NMR spectroscopy

E. coli BL21 cells expressing the Sr33$^{6-120}$ protein (see above) were grown in M9 minimal media containing ^{13}C-labelled glucose, and ^{15}N-labelled ammonium chloride. Protein expression was induced using 1 mM IPTG (isopropyl β-D-1-thiogalactopyranoside) at 20˚C for overnight protein expression. The ^{13}C/^{15}N-labelled Sr33$^{6-120}$ protein was purified using nickel affinity and size-exclusion chromatography as described above.

The correlation time of the protein was estimated based on transverse relaxation rates (T_2), measured as described previously (1). The correlation time was converted to a molecular mass using the Stoke-Einstein equations as described in (2), using a modified equation for estimation of protein volumes according to (3) with the addition of 2 Å to account for the hydration shell.

NMR data acquisition

The ^{13}C/^{15}N-labelled Sr33$^{6-120}$ sample containing 5% D_2O was filtered using a low-protein-binding Ultrafree-MC centrifugal filter (0.22 μm pore size; Millipore, MA, USA), then 300 μL was added to a susceptibility-matched 5 mm outer-diameter microtube (Shigemi Inc., Japan).

NMR data were acquired at 25˚C using a 900 MHz AVANCE spectrometer (Bruker BioSpin, Germany) equipped with a cryogenically cooled probe. Data used for resonance assignment were acquired using non-uniform sampling (NUS); sampling schedules that approximated the rate of signal decay along the various indirect dimensions were generated using sched3D (4). The decay rates used were 1 Hz for all constant-time ^{15}N dimensions, 30 Hz for all ^{13}C dimensions, and 15 Hz for the semi-constant indirect ^{1}H dimension. ^{13}C- and ^{15}N-edited HSQC-NOESY experiments were acquired using linear sampling. Separate experiments were acquired for the aliphatic and aromatic regions of the ^{13}C dimension.

NUS data were processed using the Rowland NMR toolkit (www.rowland.org/rnmrtk/toolkit.html); maximum entropy parameters were selected automatically as described previously (5). NMR spectra were analyzed and assigned using the program CcpNmr (6). ^{1}HN, ^{15}N, ^{13}C backbone resonance assignments were obtained from the analysis of amide-proton strips in 3D HNCACB, CBCA(CO)NH, and HNCO spectra. Sidechain ^{1}H and ^{13}C chemical shifts were obtained primarily from 3D

H(CC)(CO)NH-TOCSY and (H)CC(CO)NH-TOCSY spectra, respectively. The remaining side-chain assignments were derived from 3D H(C)CH-TOCSY and ^{15}N- and ^{13}C-edited NOESY-HSQC spectra

NMR structure determination

Distance restraints for structure calculations were derived from 3D ^{13}C- and ^{15}N-edited NOESY-HSQC spectra acquired with a mixing time of 120 ms. NOESY spectra were manually peak-picked and integrated using the box-sum method in CcpNmr. The peak lists were then assigned and an ensemble of structures calculated automatically using the torsion angle dynamics package CYANA (7). The tolerances used in the structure calculations were 0.03 ppm in the indirect ^{1}H dimension, 0.02 ppm in the direct ^{1}H dimension, 0.2 ppm for the aromatic ^{13}C and ^{15}N dimensions, and 0.4 ppm for the aliphatic ^{13}C data.

Backbone dihedral-angle restraints (112 for both ϕ and ψ) were derived from TALOS+ chemical shift analysis (8); the restraint range was set to twice the estimated standard deviation. All X-Pro peptide bonds were clearly identified as *trans* on the basis of characteristic NOEs and the C_β and C_γ chemical shifts for the Pro residues.

CYANA was used to calculate 200 structures from random starting conformations, then the 20 conformers with the lowest CYANA target function were chosen to represent the structural ensemble. During the automated NOESY assignment/structure calculation process CYANA assigned 94.4% of all NOESY crosspeaks (3186 out of 3372) for Sr33.

Analytical size-exclusion chromatography (SEC) and cross-linking

The purified MLA10$^{5\text{-}120}$, Sr33$^{6\text{-}120}$ and Rx$^{1\text{-}122}$ protein (450 μg) was separated on a Superdex 75 10/300 GL SEC column with a mobile phase consisting of 10 mM HEPES pH 7.5 and 150 mM NaCl. Protein size markers chymotrypsin (25 kDa) and cytochrome c (15 kDa) were separated using the same conditions as for MLA10$^{5\text{-}120}$. Cross-linking experiments were performed as described in (9). In brief, 20 μL of MLA10$^{5\text{-}120}$ (in the SEC buffer) at a concentration of 150 μM was mixed with 5 μL of BS3 (bis(sulfosuccinimidyl)suberate) at a concentration of 20 mM. The reaction was incubated on ice and monitored at various time points from 0-120 minutes. The reaction was quenched with equal volumes of 1 M Tris pH 7.5, before the samples were separated using 13% SDS-PAGE.

Size-exclusion chromatography (SEC)-coupled multi-angle light scattering (MALS)

SEC-MALS was performed using an in-line Superdex 200 100/300 GL or Superdex 200 Increase 5/150 GL SEC column (GE Healthcare) combined with a Dawn Heleos II 18-angle light-scattering detector coupled with an Optilab TrEX refractive index detector (Wyatt Technology, Santa Barbara, CA, USA). Purified proteins were separated at 0.5 mL/min (10/300) or 0.25 mL/min (5/150) in 10 mM HEPES pH 8.0 and 150 mM NaCl. Molecular-mass calculations were performed using the Astra6.1 software (Wyatt Technology). Input of the refractive increment (dn/dc values) was set at 0.186 in the molecular-mass calculations, based on the premise that dn/dc is constant for unmodified proteins (10). The molecular mass was determined across the protein elution peak.

Size-exclusion chromatography (SEC)-coupled small-angle X-ray scattering (SAXS)

SEC-SAXS was performed during two shifts at the SAXS/WAXS beamline of the Australian Synchrotron on a Pilatus 1M detector, using an in-line WTC-030S5 SEC column and a 2 mL WTC-030S5G pre-column (Wyatt Technology), together with a Prominence modular HPLC system (Shimadzu Scientific Instruments). All experiments were conducted at 16°C using 10 mM HEPES (pH 7.5), 150 mM NaCl buffer with 1 mM DTT. Eluate from the column was directed through a 1 mm quartz capillary mounted in the beam. For all samples, the injected volume was 95 µL at 30 mg/mL protein concentration, as determined by UV absorbance at 280 nm. High concentrations were used to maximize signal after dilution during gel-filtration, as the expected particle size is small.

The data for Sr33 was collected in 5 s exposures at 0.05 s intervals with a flow rate of 0.25 mL/min. A Wyatt WTC-030S5G pre-column was used upstream of the WTC-030S5. The sample-to-detector distance was 1.6 m, and a wavelength of 1.12713 Å yielded a range of momentum transfer ($0.009 < q < 0.478$ Å^{-1}, where $q = 4\pi.\sin(\theta)/\lambda$). The data for MLA10$^{5\text{-}120}$ and Rx$^{1\text{-}122}$ were collected during a different shift, in 2 s exposures at 0.05 s intervals, with a flow rate of 0.5 mL/min. The WTC-030S5 without pre-column was used for these samples. A sample-to-detector distance of 1.4 m was used to obtain data over the range $0.010 < q < 0.614$ Å^{-1}.

Data reduction, normalisation and subtraction was performed using scatterBrain (http://www.synchrotron.org.au/index.php/aussyncbeamlines/saxswaxs/software-saxswaxs). Unless noted otherwise, subsequent analyses were performed using the tools in version 2.6 of the ATSAS program suite (11).

100 frames immediately preceding each peak were summed and normalized for exposure time to obtain buffer blanks. Initially, these buffers were subtracted from each

individual image to generate a series of subtracted frames across the elution peak, from which $I(0)$ and R_g were individually calculated using the Guinier approximation, as implemented in batch-mode AUTORG, for points such that $q.R_g$ <1.3. Molecular masses were calculated using a local high-throughput implementation of the volume of correlation (V_c) method developed by Rambo and Tainer (12), for points up to q = 0.3.

These metrics were evaluated for variation across the peak. To obtain the final scattering curves for analysis, the original images from elution ranges corresponding to the peak centre and the peak tail, were summed and normalized in scatterBrain, and then subtracted from the corresponding blank.

Guinier analysis and the determination of $I(0)$, R_g and MM_{Vc} were performed on the summed and averaged curves in the same manner as for individual frames. Data-points closer to the beamstop than the first Guinier point were discarded. Data points where q > 0.46 Å^{-1} were also discarded, due to poor signal-to-noise. Distance distributions, *P(r)*, were obtained by indirect transformation in GNOM (https://www.embl-hamburg.de/biosaxs/gnom.html), informed by AUTOGNOM. In addition to MM_{Vc}, molecular masses were also estimated from the Porod volume calculated by GNOM, using the empirical ratio developed by Pethoukhov and coworkers of $MM_{Porod} = V_{Porod}*0.625$ (11).

Theoretical scattering was calculated from atomic models using FoXS (13). Short stretches of residues not visible in the electron density of the published MLA10$^{5\text{-}120}$ crystal structure were added to both chains using the loop-building routines in MODELLER (14) independently from the SAXS data.

Crystallization and crystal structure determination of MLA10$^{5\text{-}120}$

Native and selenomethionine-labelled MLA10$^{5\text{-}120}$ protein at 10 mg/mL and 6 mg/mL, respectively, in 10 mM HEPES (pH 8.0), 100 mM NaCl, and 1 mM DTT were used in crystallization trials. Crystallization experiments were initially performed with native protein using hanging-drop vapour diffusion in 96-well plates. Several commercial screens were used, including Index, PEG/Ion and PEGRx (Hampton Research) and Pact Premier and JCSG+ (Molecular Dimensions). 100 nl protein solution and 100 nl well solution were prepared on hanging-drop seals (TTP4150-5100 sourced from Millennium Science, Australia) using a Mosquito robot (TTP Lab-Tech, UK) and equilibrated against 75 ml reservoir solution. The drops were monitored and imaged using the Rock Imager system (Formulatrix, USA). Numerous promising hits were observed within 24 hours; however, the crystals grown in Pact Premier, condition B4 (MIB buffer pH 7.0, 25% PEG 1500) were pursued for data collection. Crystals grown in

larger 1:1 μL (protein: well solution) drops were cryo-protected using the well-solution containing 20% glycerol prior to flash-cooling in liquid nitrogen. X-ray diffraction data of the native crystals were collected from a single crystal at the Australian Synchrotron MX2 beamline to ~2.0 Å resolution using a wavelength of 0.9537 Å. The crystal-to-detector distance was set to 200 mm and the oscillation range was 0.5°. Data collection was performed using Blu-Ice software, indexed and integrated using XDS (15) and scaled with AIMLESS within the CCP4 suite (16). With the native data-set molecular replacement was attempted using the published MLA10$^{5\text{-}120}$ structure (PDB ID 3QFL; (9)) in monomeric, dimeric and various truncated forms, as well as the structure of Rx$^{1\text{-}122}$ (PDB ID 4M70; (17)); however, a solution could not be obtained. Subsequently, selenomethionine-labelled protein (confirmed by mass spectrometry) was crystallized as described for the native protein. X-ray diffraction data of selenomethionine-labelled crystals were collected from a single crystal at the Australian Synchrotron MX2 beamline to ~2.1 Å resolution using a wavelength 0.9792 Å. The crystal-to-detector distance was set to 200 mm and the oscillation range was 0.5°. Data collection was performed using Blu-Ice software, indexed and integrated using XDS (15) and scaled with AIMLESS within the CCP4 suite (16).

The crystals of MLA10$^{5\text{-}120}$ appeared to have the symmetry of the space group $P22_12_1$ and the structure was solved using single-wavelength anomalous diffraction (SAD) through the CRANK2 pipeline (18). Model building and refinement was done through cycles of Coot (19) and refinement in BUSTER-TNT (20). Refinement, however, proved unstable with BUSTER-TNT, unable to converge on a stable anisotropy ratio. Furthermore, R_{work} and R_{free} would stall at ~28% and ~30%, respectively. These factors could be improved by expanding the R_{free} test set from $P22_12_1$ to P1 space groups, and reprocessing the data to the P1 space group. In addition, we combined direct interactive modeling using interactive molecular dynamics flexible fitting (iMDFF) in VMD (21) and Phenix.refine (22) to generate the final model. Statistics for the refined atomic model are presented in Table S4.

Constructs for *in planta* analyses

Details of primers and constructs used in this study are given in Table S6 and S7. For transient expression in *N. benthamiana*, molecular cloning was performed by a combination of Quikchange site-directed mutagenesis (Agilent Technologies) and Gateway recombination (Life Technologies) as detailed in Table S7. The MLA10$_{1\text{-}160}$, Sr33$_{1\text{-}160}$ and Sr50$_{1\text{-}163}$ constructs cloned in pDONR207 (29) were used as templates for site-directed deletion to generate the MLA10$_{1\text{-}130}$, MLA10$_{1\text{-}135}$, MLA10$_{1\text{-}141}$, MLA10$_{1\text{-}142}$, MLA10$_{1\text{-}144}$, MLA10$_{1\text{-}148}$, Sr33$_{1\text{-}130}$, Sr33$_{1\text{-}135}$, Sr33$_{1\text{-}141}$, Sr33$_{1\text{-}142}$, Sr33$_{1\text{-}144}$, Sr33$_{1\text{-}148}$, Sr50$_{1\text{-}}$

$_{133}$, $Sr50_{1-138}$, $Sr50_{1-144}$, $Sr50_{1-145}$, $Sr50_{1-147}$ and $Sr50_{1-151}$ ENTRY constructs. These constructs were then recombined by LR reaction in the binary vector pBIN19-35S::GTW:3HA or pBIN19-35S::GTW:CFP by LR coning to obtain expression vectors.

Transient protein expression and cell death assays in *N. benthamiana*

N. benthamiana plants were grown in a growth chamber at 23°C with a 16 hours light period. For *N. benthamiana* leaf transformations, pBIN19-derived vector constructs were transformed into *Agrobacterium tumefaciens* strain GV3101_pMP90. Bacterial strains were grown in Luria-Bertani liquid medium containing 50 mg/ml rifampicin, 15 mg/ml gentamycin and 25 mg/ml kanamycin at 28°C for 24 hours. Bacteria were harvested by centrifugation, resuspended in infiltration medium (10 mM MES pH 5.6, 10 mM $MgCl_2$ and 150 µM acetosyringone) to an OD_{600nm} ranging from 0.5 to 1, and incubated for 2 hours at room temperature before leaf infiltration. Three leaves from two plants were infiltrated for each combination of constructs and the experiment was repeated three times independently. The infiltrated plants were incubated in growth chambers under controlled conditions for all following assays. For documentation of cell death, leaves were scanned five days after infiltration.

Protein extraction western blot and co-immunoprecipitation

Protein extraction, from *N. benthamiana* leaves and co-IP experiments were performed as described (23). For immunoblotting analysis, proteins were separated by SDS-PAGE and transferred to a nitrocellulose membrane. Membranes were blocked in 5% skimmed milk and probed with anti-HA-HRP antibodies (Roche) or anti-GFP antibodies (Roche) followed by goat anti-mouse antibodies conjugated with horseradish peroxidase (Pierce). Labeling was detected using the SuperSignal West Femto chemiluminescence kit (Pierce). Membranes were stained with Ponceau S to confirm equal loading.

Table S1. NMR structure statistics[a]

Experimental restraints[b]	
Inter-proton distance restraints	
Intra-residue	580
Sequential	186
Medium-range (i–j < 5)	293
Long-range (i–j > 5)	249
Dihedral-angle restraints	224
Total number of restraints per residue	13.32
RMSD from the mean of the atomic coordinates of the ensemble (Å)[c]	
Backbone atoms (residues 6–89 & 98–110)	0.93 ± 0.21
All heavy atoms (residues 6–89 & 98–110)	1.31 ± 0.19
Stereochemical quality[d]	
Residues in most favoured Ramachandran region (%)	93.1
Ramachandran outliers (%)	0 ± 0
Unfavourable side-chain rotamers (%)	0 ± 0
Clashscore, all atoms[b]	0 ± 0

[a]All statistics are given as mean (some ± SD).

[b]Only structurally relevant restraints, as defined by CYANA, are included.

[c]Mean r.m.s. deviation calculated over the entire ensemble of 20 structures.

[d]As reported by CYANA (7, 24).

Table S2. Properties derived from averaged SAXS datasets

Protein	Fraction	Elution range (mL)	$I(0)_{\text{Guin}}$ (cm^{-1})	$I(0)_{P(r)}$ (cm^{-1})	$R_{g\ \text{Guin}}$ (Å)	$R_{g\ P(r)}$ (Å)	MM_{Vc} (kDa)	MM_{Porod} (kDa)
$Sr33^{6\text{-}120}$	Centre	11.77 – 12.31	4.12 e^{-2}	4.14 e^{-2}	18.84	19.55*	13.8	14.4
	Tail	12.35 – 12.69	1.28 e^{-2}	1.28 e^{-2}	17.08	17.23	13.5	11.4
$MLA10^{5\text{-}120}$	Centre	9.29 – 10.04	3.69 e^{-2}	3.76 e^{-2}	20.67	23.02*	16.0	15.6
	Tail	10.42 – 11.29	0.46 e^{-2}	0.46 e^{-2}	17.72	17.66	13.7	12.8
$Rx^{1\text{-}122}$	Centre	9.48 – 10.07	3.95 e^{-2}	4.01 e^{-2}	20.70	23.29*	16.3	15.8
	Tail	10.65 – 11.32	0.31 e^{-2}	0.31 e^{-2}	17.10	17.41	13.8	12.2

* Values for $R_{g\ P(r)}$ that differ from $R_{g\ \text{Guin}}$ by greater than 5%

The theoretical monomeric molecular masses of $Sr33^{6\text{-}120}$, $MLA10^{5\text{-}120}$ and $Rx^{1\text{-}122}$ are 13.1 kDa, 13.4 kDa and 14.3 kDa, respectively.

Table S3. Goodness-of-fit (χ) scores for averaged SAXS datasets compared to structures

Sample	Fraction	Atomic structure (PDB ID)					
		$Sr33^{6-120}$	Rx^{1-122}	$MLA10^{5-120}$			
		NMR*	4M70	3QFL monomer	3QFL dimer	MX* monomer	MX* dimer
$Sr33^{5-120}$	Tail	0.67	1.63	12.03	8.41	11.54	8.08
$MLA10^{5-120}$	Tail	0.51	0.87	3.99	2.88	3.85	2.75
Rx^{1-122}	Tail	0.48	0.73	3.44	2.71	3.41	2.58

* Structure presented in this work.

Table S4. Crystallographic table for MLA10$^{5\text{-}120}$

Data processing		
Space group	P 2 $2_1 2_1$	P 1
a, b, c (Å)	30.87, 87.56, 92.56	30.72, 87.14, 92.25
α, β, γ (°)	90, 90, 90	89.93, 90.00, 89.98
Resolution (Å)	46.28-2.1 (2.16-2.10) [a]	46.12-2.05 (2.10-2.05)
Rmeas (%) [b]	11.0 (194.0)	6.8 (79.2)
Rpim(%) [c]	3.0 (51.0)	4.8 (56.0)
<I/σ(I)>	15.0 (1.8)	8.2 (1.4)
$CC_{1/2}$ [d]	0.99 (0.89)	0.99 (0.77)
Completeness (%)	100 (100)	96.5 (92.9)
Multiplicity	14.1 (14.4)	1.8 (1.8)
Wilson plot B (Å^2)	44.7	38.9
Observations	216711 (18084)	107102 (7880)
Unique reflections	15392 (1253)	58095 (4314)
Anomalous completeness	100 (100)	-
Anomalous multiplicity	7.7 (7.7)	-
DelAnom correlation between half-sets	0.471 (-0.027)	-
Mid-slope of anomalous normal probability	1.087	-
Estimate of maximum resolution for significant anomalous signal = 3.59 Å, from CCanom > 0.15		
Refinement		
Rwork (%)	27.9 (31.1)	25.2 (37.7)
Rfree (%)	30.1 (35.0)	27.9 (40.7)
Average B-factor (Å^2)	60.35	62.15
R.m.s deviations		
Bond lengths (Å)	0.009	0.001
Bond angles (°)	1.07	0.348
Ramachandran plot (%) [e]		
Favoured	96.41	99.32
Allowed	99.10	100.00
Outliers	0.90	0.00

[a] NB: Values within parentheses indicate the highest resolution bin.
[b] $R_{meas} = \sum_{hkl}\{N(hkl)/[N(hkl)\text{-}1]\}^{1/2} \sum_i |I_i(hkl) - \langle I(hkl)\rangle| / \sum_{hkl}\sum_i I_i(hkl)$, where $I_i(hkl)$ is the intensity of the ith measurement of an equivalent reflection with indices hkl.
[c] $R_{pim} = \sum_{hkl}\{1/[N(hkl)\text{-}1]\}^{1/2} \sum_i |I_i(hkl) - \langle I(hkl)\rangle| / \sum_{hkl}\sum_i I_i(hkl)$.
[d] Calculated with the program Aimless (25).
[e] As calculated by MolProbity (26).

Table S5. Summary of predicted and experimental average molecular masses for constructs as determined by MALS.

	Theoretical Molecular Mass (kDa)		Experimental Molecular Mass (kDa)	
Construct	Monomer	Dimer	Shoulder	Main peak
$Sr33^{6\text{-}120}$	13.12	16.24	-	13.9
$Sr33^{6\text{-}144}$	15.94	31.88	27.3	17.5
$Sr33^{6\text{-}160}$	17.65	35.30	35.0	19.3
$MLA10^{5\text{-}}$	13.28	26.56	-	13.4
$MLA10^{5\text{-}}$	16.17	32.34	-	22.8

Table S6. Primers used in this study for *in-planta* and *in vitro* studies

Primer name	Primer sequence 5'-3'
oCS281	GACATCCAAGAGCAACTCGACCCAGCTTTCTTGTAC
oCS282	GTACAAGAAAGCTGGGTCGAGTTGCTCTTGGATGTC
oCS283	GCAACTCCAAAAGGTGGCTGATGACCCAGCTTTCTTGTAC
oCS284	GTACAAGAAAGCTGGGTCATCAGCCACCTTTTGGAGTTGC
oCS285	GATAGGCGTGACAGGAACAAGGACCCAGCTTTCTTGTAC
oCS286	GTACAAGAAAGCTGGGTCCTTGTTCCTGTCACGCCTATC
oCS287	TAGGCGTGACAGGAACAAGGTAGACCCAGCTTTCTTGTAC
oCS288	GTACAAGAAAGCTGGGTCTACCTTGTTCCTGTCACGCCTA
oCS289	CGTGACAGGAACAAGGTATTTGTTGACCCAGCTTTCTTGTAC
oCS290	GTACAAGAAAGCTGGGTCAACAAATACCTTGTTCCTGTCACG
oCS291	GGTATTTGTTCCTCATCCTACGGACCCAGCTTTCTTGTAC
oCS292	GTACAAGAAAGCTGGGTCCGTAGGATGAGGAACAAATACC
oCS293	GACATCAAGAAGGAACTCGACCCAGCTTTCTTGTAC
oCS294	GTACAAGAAAGCTGGGTCGAGTTCCTTCTTGATGTC
oCS295	CTCCAGGAGGTGGCTGCTGACCCAGCTTTCTTGTAC
oCS296	GTACAAGAAAGCTGGGTCAGCAGCCACCTCCTGGAG
oCS297	CTAGGCGTGACAGGAACAAGGACCCAGCTTTCTTGTAC
oCS298	GTACAAGAAAGCTGGGTCCTTGTTCCTGTCACGCCTAG
oCS299	CGTGACAGGAACAAGTTCGACCCAGCTTTCTTGTAC
oCS300	GTACAAGAAAGCTGGGTCGAACTTGTTCCTGTCACG
oCS301	AGGAACAAGTTCGATGGTGACCCAGCTTTCTTGTAC
oCS302	GTACAAGAAAGCTGGGTCACCATCGAACTTGTTCCT
oCS303	GAACAAGTTCGATGGTATTGCTTCTATTGACCCAGCTTTCTTGTAC
oCS304	GTACAAGAAAGCTGGGTCAATAGAAGCAATACCATCGAACTTGTTC
oCS305	GAAATCAAGGAGCAACTCGACCCAGCTTTCTTGTAC
oCS306	GTACAAGAAAGCTGGGTCGAGTTGCTCCTTGATTTC
oCS307	CTCCAGGAGGTGGCTGCTGACCCAGCTTTCTTGTAC
oCS308	GTACAAGAAAGCTGGGTCAGCAGCCACCTCCTGGAG
oCS309	GCTAGGCGTGACAGGAACAAGGACCCAGCTTTCTTGTAC
oCS310	GTACAAGAAAGCTGGGTCCTTGTTCCTGTCACGCCTAGC
oCS311	TAGGCGTGACAGGAACAAGGTAGACCCAGCTTTCTTGTAC
oCS312	GTACAAGAAAGCTGGGTCTACCTTGTTCCTGTCACGCCTA
oCS313	CGTGACAGGAACAAGGTAGCTGTTGACCCAGCTTTCTTGTAC
oCS314	GTACAAGAAAGCTGGGTCAACAGCTACCTTGTTCCTGTCACG
oCS315	GCTGTTCCTAATCCTATGGACCCAGCTTTCTTGTAC
oCS316	GTACAAGAAAGCTGGGTCCATAGGATTAGGAACAGC
MLA10_5_FW	TACTTCCAATCCAATGCGACCGGTGCCATTTCCAACCTGATTCC
MLA10_120_RV	TATTCCACTTCCAATGTTAAGCTATCCCATGCTTATGCTTGACTTTCTTC
MLA10_144_RV	TATTCCACTTCCAATGTTAAACAAATACCTTGTTCCTGTCACGCCTATC
MLA10_160_RV	TATTCCACTTCCAATGTTACAAAGCTC
Sr50_5_FW	TACTTCCAATCCAATGCGACGGGGGCCATGG
Sr50_123_RV	TATTCCACTTCCAATGTTAAGCTATGCGATGGTGATTC
Sr33_6_FW	TACTTCCAATCCAATGCGACGGGTGCCA
Sr33_120_RV	TATTCCACTTCCAATGTTAAGCTATTC
Sr33_144_RV	TATTCCACTTCCAATGTTAACCATCGAACTTGTTCCTGTCACGCC
Sr33_160_RV	TATCCACTTCCAATGTTATAGAGCACGG

Table S7. Constructs used in this study for *in-planta* and *in vitro* analysis

Use	Construct	Plasmid name	Insert or PCR product	Primers	Template	Plasmid backbone	Cloning method	Reference
Entry clones for *N. benthamiana* assays	MLA10$^{1-160}$	pSC260	MLA10$^{1-160}$ (without stop)	/	/	pDONR207	/	29
	Sr33$^{1-160}$	pSC298	Sr33$^{1-160}$ (without stop)	/	/	pDONR207	/	29
	Sr50$^{1-163}$	pSC262	Sr50$^{1-163}$ (without stop)	/	/	pDONR207	/	29
	MLA10$^{1-130}$	pSC392	MLA10$^{1-130}$ (without stop)	oCS281/282	pSC260	pDONR207	Quikchange lightning (Agilent)	/
	MLA10$^{1-135}$	pSC393	MLA10$^{1-135}$ (without stop)	oCS283/284	pSC260	pDONR207	Quikchange lightning (Agilent)	/
	MLA10$^{1-141}$	pSC394	MLA10$^{1-141}$ (without stop)	oCS285/286	pSC260	pDONR207	Quikchange lightning (Agilent)	/
	MLA10$^{1-142}$	pSC395	MLA10$^{1-142}$ (without stop)	oCS287/288	pSC260	pDONR207	Quikchange lightning (Agilent)	/
	MLA10$^{1-144}$	pSC396	MLA10$^{1-144}$ (without stop)	oCS289/290	pSC260	pDONR207	Quikchange lightning (Agilent)	/
	MLA10$^{1-148}$	pSC397	MLA10$^{1-148}$ (without stop)	oCS291/292	pSC260	pDONR207	Quikchange lightning (Agilent)	/
	Sr33$^{1-130}$	pSC398	Sr33$^{1-130}$ (without stop)	oCS293/294	pSC298	pDONR207	Quikchange lightning (Agilent)	/
	Sr33$^{1-135}$	pSC399	Sr33$^{1-135}$ (without stop)	oCS295/296	pSC298	pDONR207	Quikchange lightning (Agilent)	/
	Sr33$^{1-141}$	pSC400	Sr33$^{1-141}$ (without stop)	oCS297/298	pSC298	pDONR207	Quikchange lightning (Agilent)	/
	Sr33$^{1-142}$	pSC401	Sr33$^{1-142}$ (without stop)	oCS299/300	pSC298	pDONR207	Quikchange lightning (Agilent)	/
	Sr33$^{1-144}$	pSC402	Sr33$^{1-144}$ (without stop)	oCS301/302	pSC298	pDONR207	Quikchange lightning (Agilent)	/
	Sr33$^{1-148}$	pSC403	Sr33$^{1-148}$ (without stop)	oCS303/304	pSC298	pDONR207	Quikchange lightning (Agilent)	/
	Sr50$^{1-133}$	pSC404	Sr50$^{1-133}$ (without stop)	oCS305/306	pSC262	pDONR207	Quikchange lightning (Agilent)	/
	Sr50$^{1-138}$	pSC405	Sr50$^{1-138}$ (without stop)	oCS307/308	pSC262	pDONR207	Quikchange lightning (Agilent)	/
	Sr50$^{1-144}$	pSC406	Sr50$^{1-144}$ (without stop)	oCS309/310	pSC262	pDONR207	Quikchange lightning (Agilent)	/
	Sr50$^{1-145}$	pSC407	Sr50$^{1-145}$ (without stop)	oCS311/312	pSC262	pDONR207	Quikchange lightning (Agilent)	/
	Sr50$^{1-147}$	pSC408	Sr50$^{1-147}$ (without stop)	oCS313/314	pSC262	pDONR207	Quikchange lightning (Agilent)	/
	Sr50$^{1-151}$	pSC409	Sr50$^{1-151}$ (without stop)	oCS315/316	pSC262	pDONR207	Quikchange lightning (Agilent)	/
Cell death assays and co-IPs in *N. benthamiana*	RGA4$^{1-171}$:CFP	pSC167	RGA4$^{1-171}$	/	/	pBin19-35s::GTW:CFP	/	17
	MLA10$^{1-160}$:CFP	pSC302	MLA10$^{1-160}$	/	/	pBin19-35s::GTW:CFP	/	29
	Sr33$^{1-160}$:CFP	pSC301	Sr33$^{1-160}$	/	/	pBin19-35s::GTW:CFP	/	29
	Sr50$^{1-163}$:HA	pSC280	Sr50$^{1-163}$	/	/	pBin19-35s::GTW:HA	/	29
	Sr50$^{1-163}$:CFP	pSC303	Sr50$^{1-163}$	/	/	pBin19-35s::GTW:CFP	/	29
	MLA10$^{1-130}$:HA	pSC410	MLA10$^{1-130}$	/	pSC392	pBin19-35s::GTW:HA	LR Gateway (Life Technologies)	/
	MLA10$^{1-135}$:HA	pSC411	MLA10$^{1-135}$	/	pSC393	pBin19-35s::GTW:HA	LR Gateway (Life Technologies)	/
	MLA10$^{1-141}$:HA	pSC412	MLA10$^{1-141}$	/	pSC394	pBin19-35s::GTW:HA	LR Gateway (Life Technologies)	/
	MLA10$^{1-142}$:HA	pSC413	MLA10$^{1-142}$	/	pSC395	pBin19-35s::GTW:HA	LR Gateway (Life Technologies)	/
	MLA10$^{1-144}$:HA	pSC414	MLA10$^{1-144}$	/	pSC396	pBin19-35s::GTW:HA	LR Gateway (Life Technologies)	/
	MLA10$^{1-148}$:HA	pSC415	MLA10$^{1-148}$	/	pSC397	pBin19-35s::GTW:HA	LR Gateway (Life Technologies)	/

	$Sr33^{1-130}$:HA	pSC416	$Sr33^{1-130}$	/	pSC398	pBin19-35s::GTW:HA	LR Gateway (Life Technologies)	/
	$Sr33^{1-135}$:HA	pSC417	$Sr33^{1-135}$	/	pSC399	pBin19-35s::GTW:HA	LR Gateway (Life Technologies)	/
	$Sr33^{1-141}$:HA	pSC418	$Sr33^{1-141}$	/	pSC400	pBin19-35s::GTW:HA	LR Gateway (Life Technologies)	/
	$Sr33^{1-142}$:HA	pSC419	$Sr33^{1-142}$	/	pSC401	pBin19-35s::GTW:HA	LR Gateway (Life Technologies)	/
	$Sr33^{1-144}$:HA	pSC420	$Sr33^{1-144}$	/	pSC402	pBin19-35s::GTW:HA	LR Gateway (Life Technologies)	/
	$Sr33^{1-148}$:HA	pSC421	$Sr33^{1-148}$	/	pSC403	pBin19-35s::GTW:HA	LR Gateway (Life Technologies)	/
	$Sr50^{1-133}$:HA	pSC422	$Sr50^{1-133}$	/	pSC404	pBin19-35s::GTW:HA	LR Gateway (Life Technologies)	/
	$Sr50^{1-138}$:HA	pSC423	$Sr50^{1-138}$	/	pSC405	pBin19-35s::GTW:HA	LR Gateway (Life Technologies)	/
	$Sr50^{1-144}$:HA	pSC424	$Sr50^{1-144}$	/	pSC406	pBin19-35s::GTW:HA	LR Gateway (Life Technologies)	/
	$Sr50^{1-145}$:HA	pSC425	$Sr50^{1-145}$	/	pSC407	pBin19-35s::GTW:HA	LR Gateway (Life Technologies)	/
	$Sr50^{1-147}$:HA	pSC426	$Sr50^{1-147}$	/	pSC408	pBin19-35s::GTW:HA	LR Gateway (Life Technologies)	/
	$Sr50^{1-151}$:HA	pSC427	$Sr50^{1-151}$	/	pSC409	pBin19-35s::GTW:HA	LR Gateway (Life Technologies)	/
	$MLA10^{1-141}$:CFP	pSC428	$MLA10^{1-141}$	/	pSC394	pBin19-35s::GTW:CFP	LR Gateway (Life Technologies)	/
	$MLA10^{1-142}$:CFP	pSC429	$MLA10^{1-142}$	/	pSC395	pBin19-35s::GTW:CFP	LR Gateway (Life Technologies)	/
	$MLA10^{1-144}$:CFP	pSC430	$MLA10^{1-144}$	/	pSC396	pBin19-35s::GTW:CFP	LR Gateway (Life Technologies)	/
	$Sr33^{1-141}$:CFP	pSC431	$Sr33^{1-141}$	/	pSC400	pBin19-35s::GTW:CFP	LR Gateway (Life Technologies)	/
	$Sr33^{1-142}$:CFP	pSC432	$Sr33^{1-142}$	/	pSC401	pBin19-35s::GTW:CFP	LR Gateway (Life Technologies)	/
	$Sr33^{1-144}$:CFP	pSC433	$Sr33^{1-144}$	/	pSC402	pBin19-35s::GTW:CFP	LR Gateway (Life Technologies)	/
	$Sr50^{1-144}$:CFP	pSC434	$Sr50^{1-144}$	/	pSC406	pBin19-35s::GTW:CFP	LR Gateway (Life Technologies)	/
	$Sr50^{1-145}$:CFP	pSC435	$Sr50^{1-145}$	/	pSC407	pBin19-35s::GTW:CFP	LR Gateway (Life Technologies)	/
	$Sr50^{1-147}$:CFP	pSC436	$Sr50^{1-147}$	/	pSC408	pBin19-35s::GTW:CFP	LR Gateway (Life Technologies)	/
Recombinant expression of proteins in *E. coli.*	$MLA10^{5-120}$	pMCSG7	$MLA10^{5-120}$	MLA10_5_FW / MLA10_120_RV	/	pMCSG7	Ligation-independent cloning	1
	$MLA10^{5-144}$	pMCSG7	$MLA10^{5-144}$	MLA10_5_FW / MLA10_144_RV	/	pMCSG7	Ligation-independent cloning	1
	$MLA10^{5-160}$	pMCSG7	$MLA10^{5-160}$	MLA10_5_FW / MLA10_160_RV	/	pMCSG7	Ligation-independent cloning	1
	$Sr33^{6-120}$	pMCSG7	$Sr33^{6-120}$	Sr33_6_FW / Sr33_120_RV	/	pMCSG7	Ligation-independent cloning	1
	$Sr33^{6-144}$	pMCSG7	$Sr33^{6-144}$	Sr33_6_FW / Sr33_144_RV	/	pMCSG7	Ligation-independent cloning	1
	$Sr33^{6-160}$	pMCSG7	$Sr33^{6-160}$	Sr33_6_FW / Sr33_160_RV	/	pMCSG7	Ligation-independent cloning	1
	$Sr50^{5-123}$	pMCSG7	$Sr50^{5-123}$	Sr50_5_FW / Sr33_123_RV	/	pMCSG7	Ligation-independent cloning	1
	Rx^{1-122}	pMCSG7	Rx^{1-122}	/		pMCSG7	Ligation-independent cloning	1

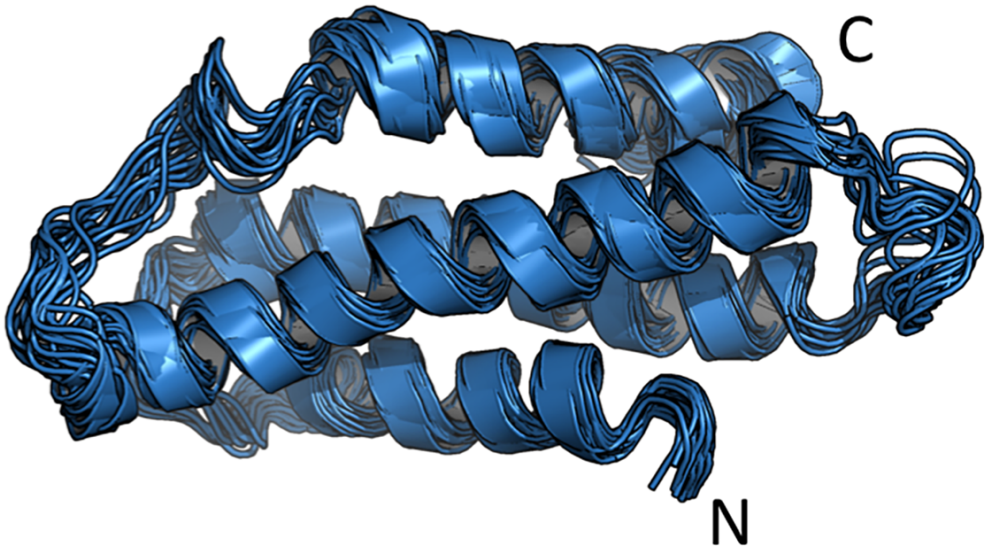

Fig. S1. Twenty superimposed lowest-energy structures of $Sr33^{6\text{-}120}$ (PDB ID 2NCG).

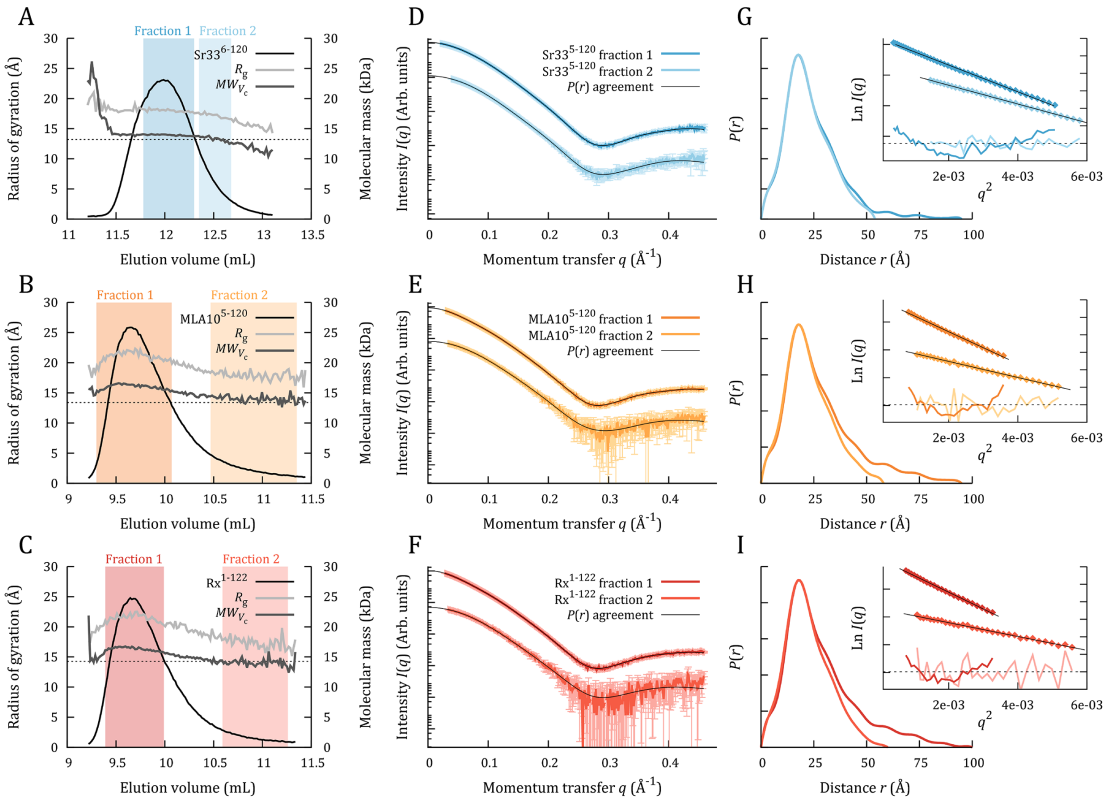

Fig. S2. Analysis of scattering curves averaged over the peak centre and dilute fractions from SEC-SAXS. (**A-C**) Evolution of particle Guinier R_g and molecular mass during in-line SEC-SAXS. For all proteins, the trace of zero-angle intensity, $I(0)$, is plotted as a black line arbitrarily scaled against the y axis, while the properties R_g and MM_{VC} are plotted as light and dark grey lines, respectively. The predicted monomeric molecular mass of each construct is shown as a black dotted line. Fractions averaged for analysis are marked by coloured shading. Note that the use of a 2 mL pre-column for Sr33$^{6\text{-}120}$ shifts that peak by the corresponding volume. (**D-F**) Experimental data-sets plotted as coloured lines, with experimental errors displayed at 1σ in lighter colour. Solid black lines indicate the fit of the corresponding distance distribution. The data-sets are arbitrarily offset along the *y*-axis for ease of visualization. (**G-I**) Normalized distance distribution functions, $P(r)$, are shown as coloured lines matching the scattering curve from which they were calculated. $P(r)$s have been normalized to reciprocal-space zero-angle intensity. The Guinier regions of the data-sets are shown in the insets, transformed as q^2 vs ln $I(q)$. Individual data-points are plotted as coloured diamonds, and a linear regression fit to each is shown as a black line. The data-sets are again offset in *y* for visualization. The residuals of each linear fit are also shown as coloured lines, plotted against the right hand axis. Aggregation in the peak fractions is apparent as a "smiling" curvature in the residuals., while the tail fraction residuals are normally distributed.

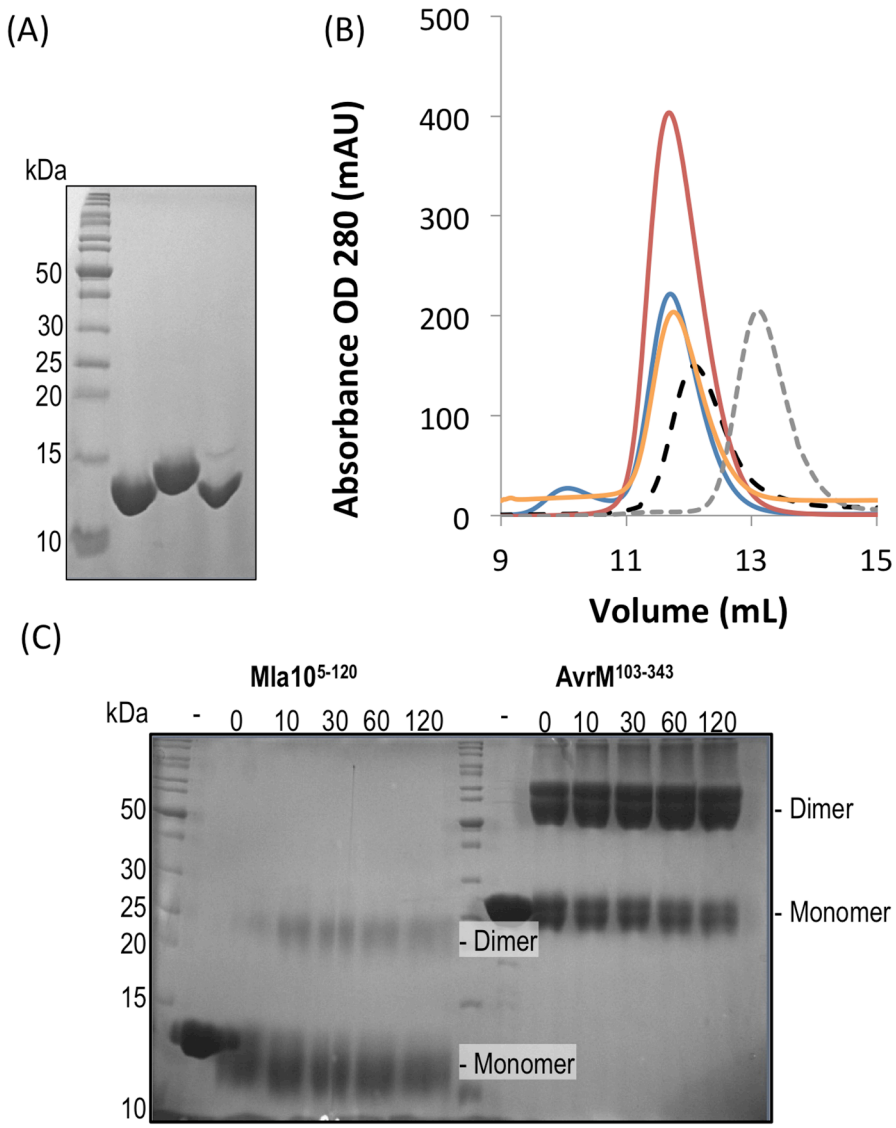

Fig. S3. Purification and SEC analysis **(A)** Coomassie blue-stained SDS-PAGE of purified (left-right) MLA10$^{5\text{-}120}$, Rx$^{1\text{-}122}$ and Sr33$^{6\text{-}120}$ proteins. **(B)** MLA10$^{5\text{-}120}$ (orange), Rx$^{1\text{-}122}$ (red) and Sr33$^{6\text{-}120}$ (blue) were separated on a Superdex S75 10/300 size-exclusion chromatography column and compared with known standards chymotrypsin (25 kDa – black dashed line) and cytochrome c (12 kDa – grey dashed line). **(C)** Chemical crosslinking of MLA10$^{5\text{-}120}$ and AvrM$^{103\text{-}343}$. The protein was incubated with the cross-linker BS3 and sampled at time points 0, 10, 30, 60, 120 min (- represents the protein without BS3 added). The protein samples were separated by SDS-PAGE and Coomassie blue-stained.

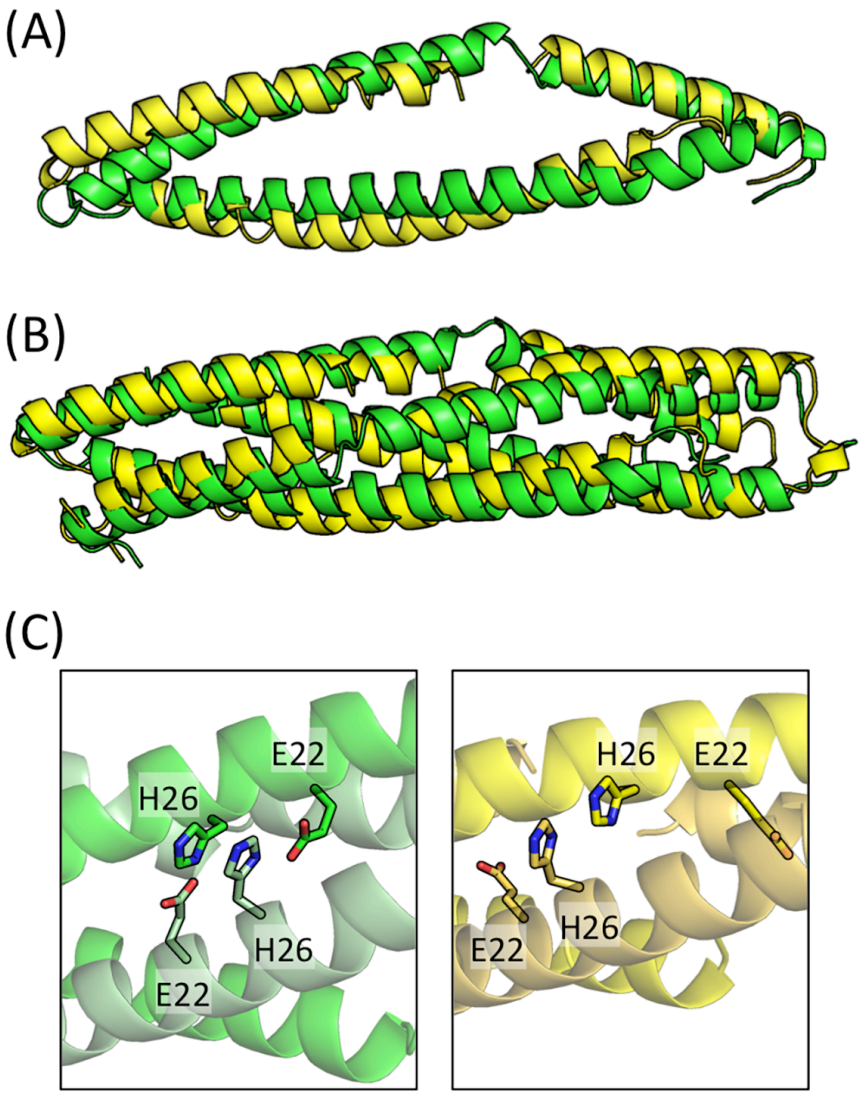

Fig. S4. A comparison of the MLA10$^{5\text{-}120}$ crystal structure solved in this study (PDB 5T1Y, shown in green) to that solved previously (9) (PDB ID 3QFL, shown in yellow). The RMSD for the monomer (**A**) and crystallographic dimer (**B**) is 3.6 Å and 3.7 Å, respectively. While overall the structures look similar there are differences between them with respect to the interactions between residues that coordinate the crystallographic dimer. (**C**) For example, in the structure solved here H26 and E22 from different protomers form a hydrogen bond (green, left), yet they do not interact in the 3QFL crystallographic dimer (yellow, right).

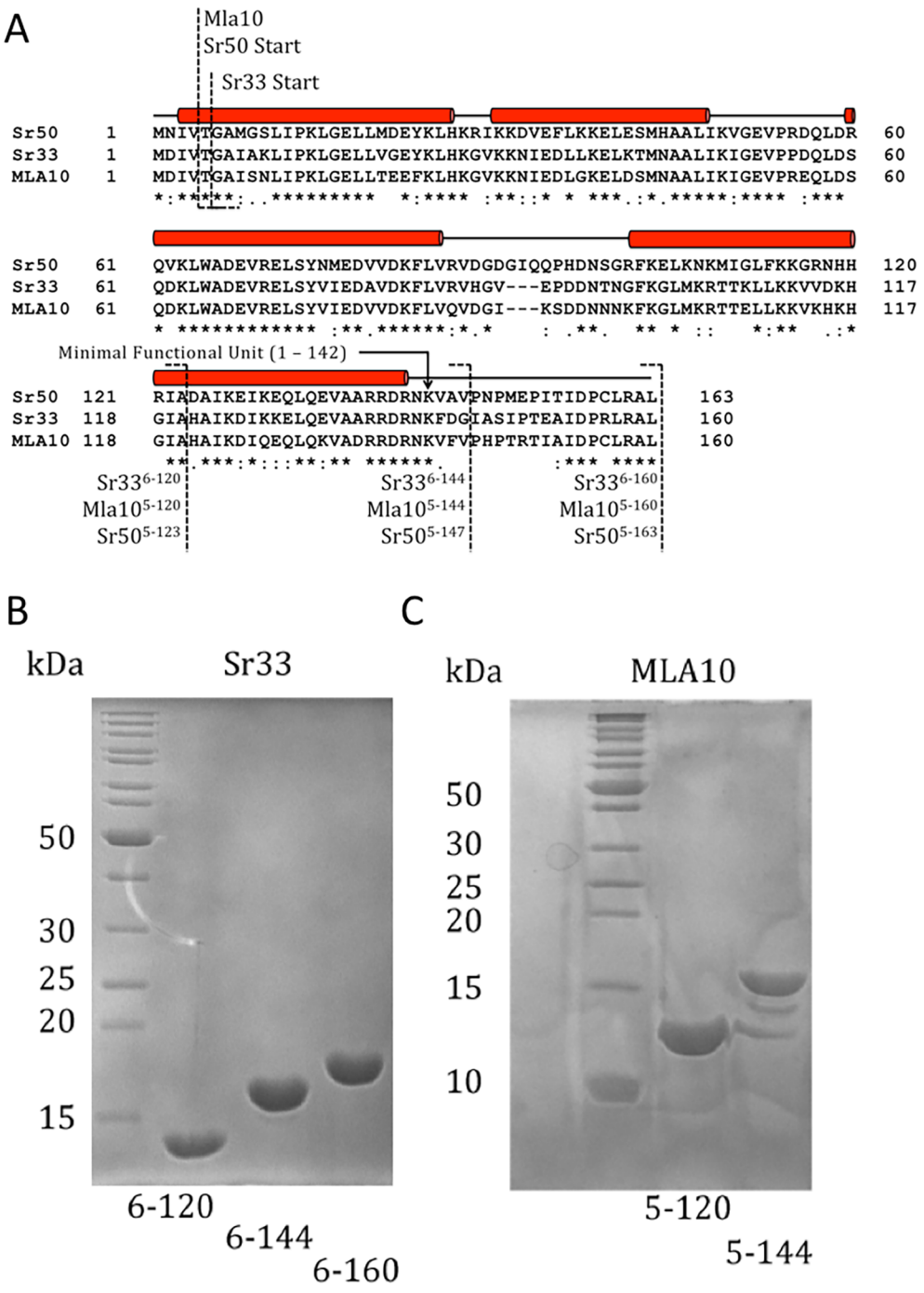

Fig. S5. Secondary structure prediction for MLA10, Sr33 and Sr50 CC domains from protein sequences using PSIPRED (27). Construct boundaries are marked with dashed lines. The minimal functional units for these constructs are indicated with an arrow. (**B, C**) Coomasie blue-stained SDS-PAGE of purified (left to right) $Sr33^{6\text{-}120}$, $Sr33^{6\text{-}144}$ and $Sr33^{6\text{-}160}$ (**B**); and $MLA10^{5\text{-}120}$ and $MLA10^{5\text{-}144}$ (**C**) proteins, used in solution studies (**Fig. 4**).

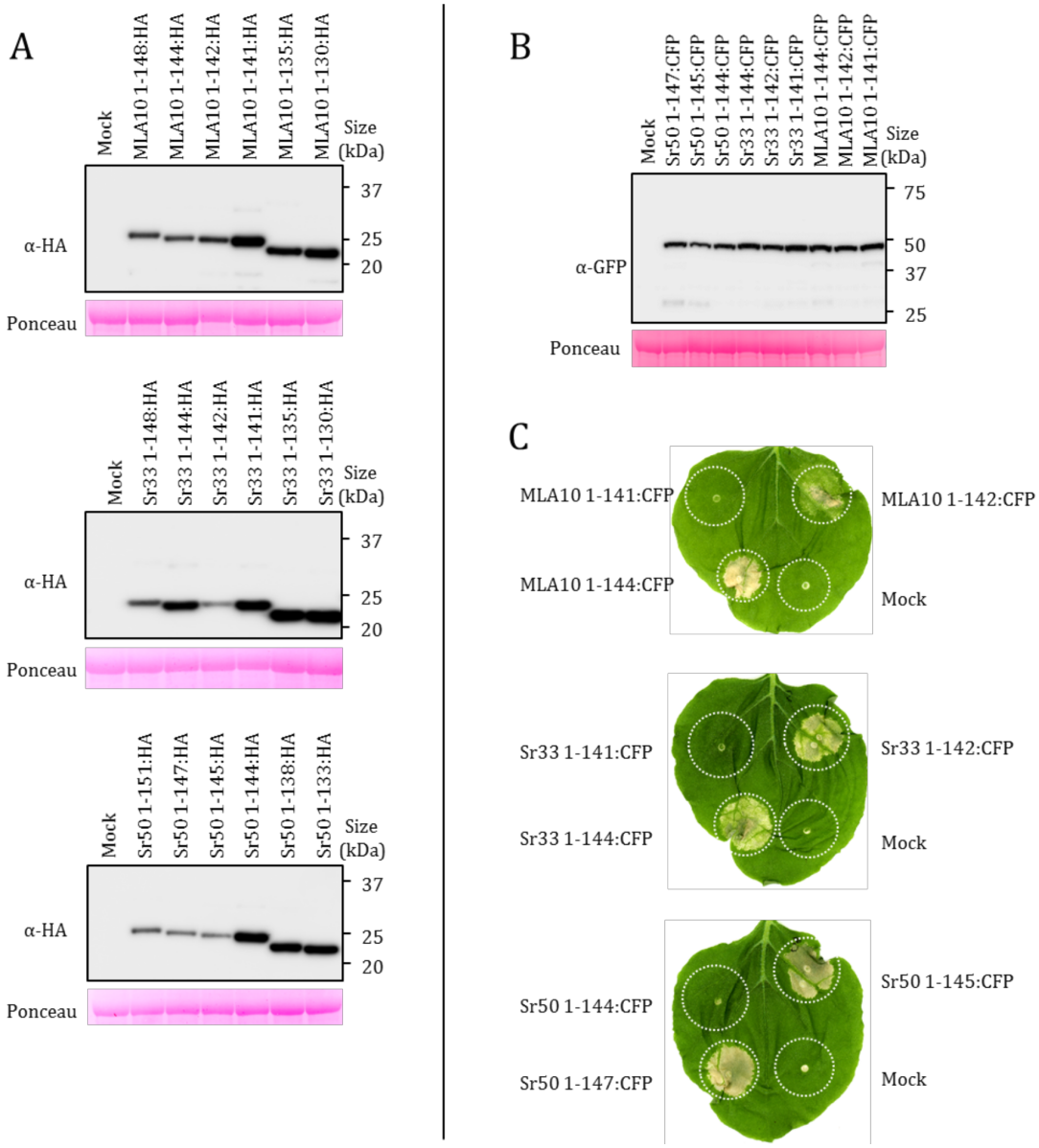

Fig. S6. HA and CFP-tagged CC fragments of MLA10, Sr33 and Sr50 expressed in *N. benthamiana*. **(A, B)** The indicated proteins were extracted from transiently transformed *N. benthamiana* leaves 20 hours after infiltration and were analyzed by immunoblotting with anti-GFP or anti-HA antibodies. Ponceau staining of RuBisCO was used to verify equal protein loading. **(C)** The indicated constructs were transiently expressed in *N. benthamiana*. Cell death was visualized five days after infiltration.

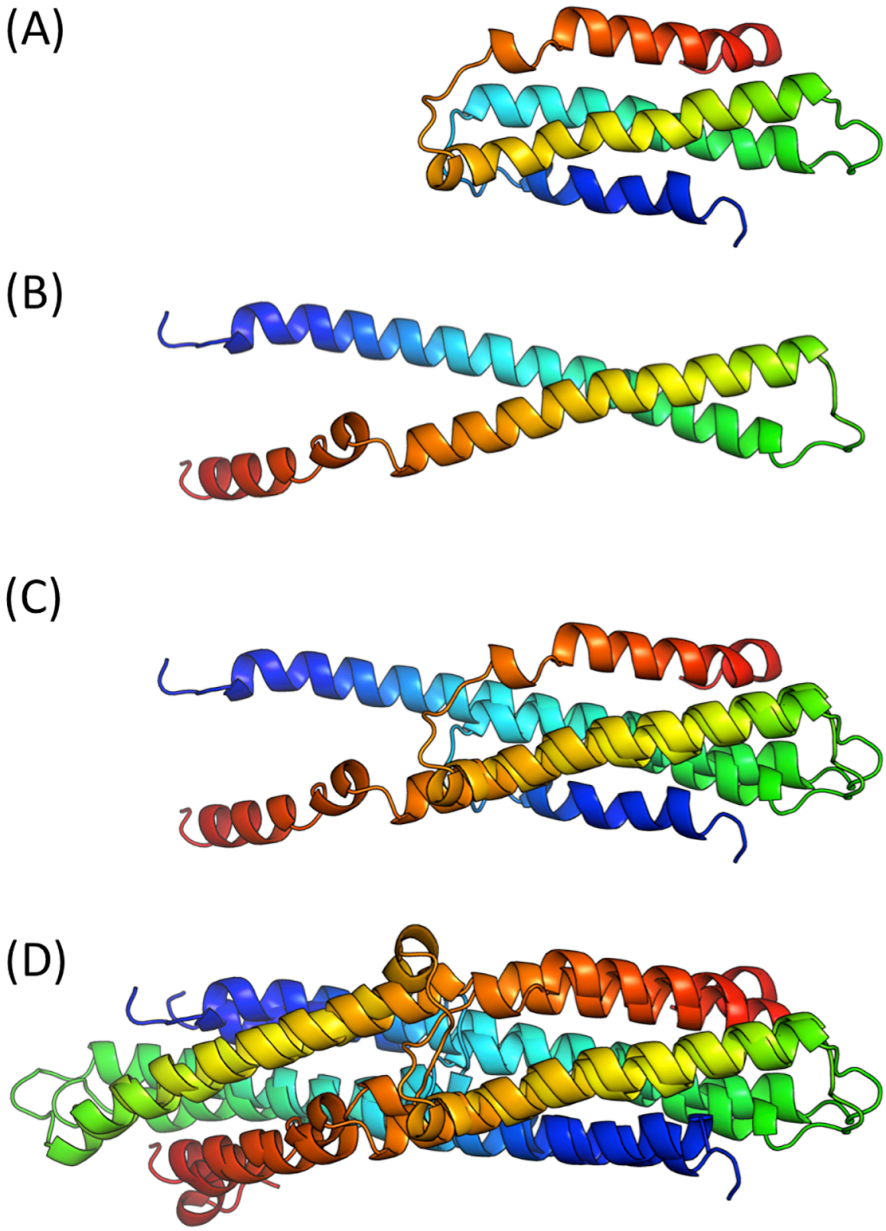

Fig. S7. Comparison of the MLA10$^{5\text{-}120}$ crystal structure and the Sr33$^{6\text{-}120}$ solution structure and the rationales' for the dimer of MLA10$^{5\text{-}120}$ representing a crystallisation induced domain-swapped dimer. (**A**) and (**B**) represent the NMR structure of Sr33$^{6\text{-}120}$ (PDB 2NCG) and the crystal structure of MLA10$^{5\text{-}120}$ (PDB 5T1Y), respectively. These are shown in cartoon and coloured using a rainbow spectrum (blue: N-terminus – red: C-terminus). Superposition of Sr33$^{6\text{-}120}$ onto MLA10$^{5\text{-}120}$ monomer (**C**) and dimer (**D**) (in (D) two Sr33 molecules were superimposed).

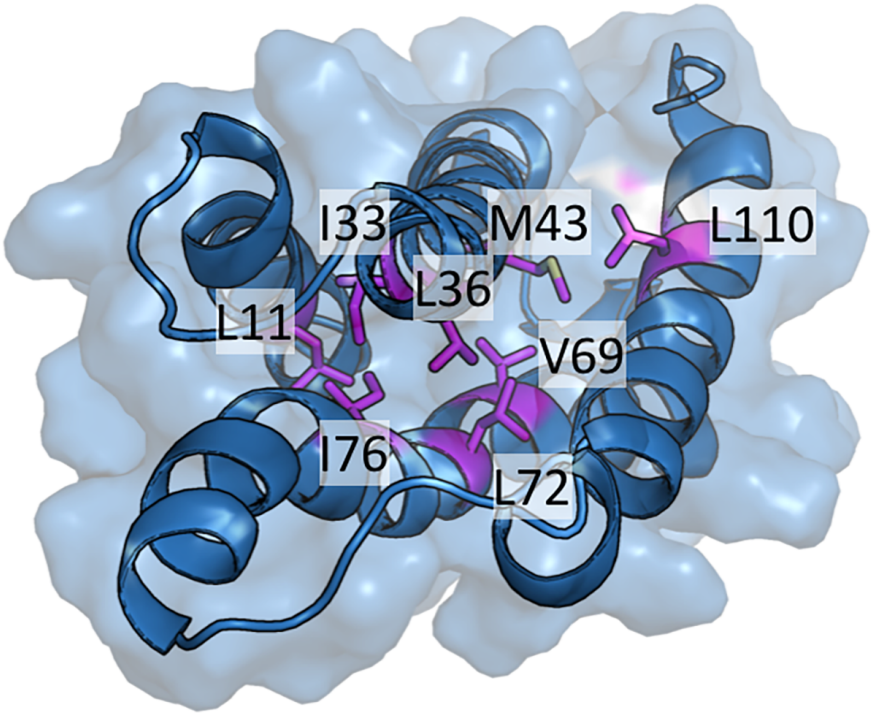

Fig. S8. Maekawa et al (9) reported that mutations in MLA10$^{5\text{-}120}$, including L11E, I33E, L36E, M43E, V69E, L72E, I76E, and L110E, could not be produced in a stable and soluble form when expressed in *E. coli*. Here the equivalent mutations are indicated in the Sr33$^{6\text{-}120}$ structure in stick representation, colored magenta and labelled. These residues form part of the four-helix bundle hydrophobic core in the Sr33$^{6\text{-}120}$ monomer. We suggest that glutamate mutations at these positions would have a destabilizing effect on the CC domain four-helix bundle fold.

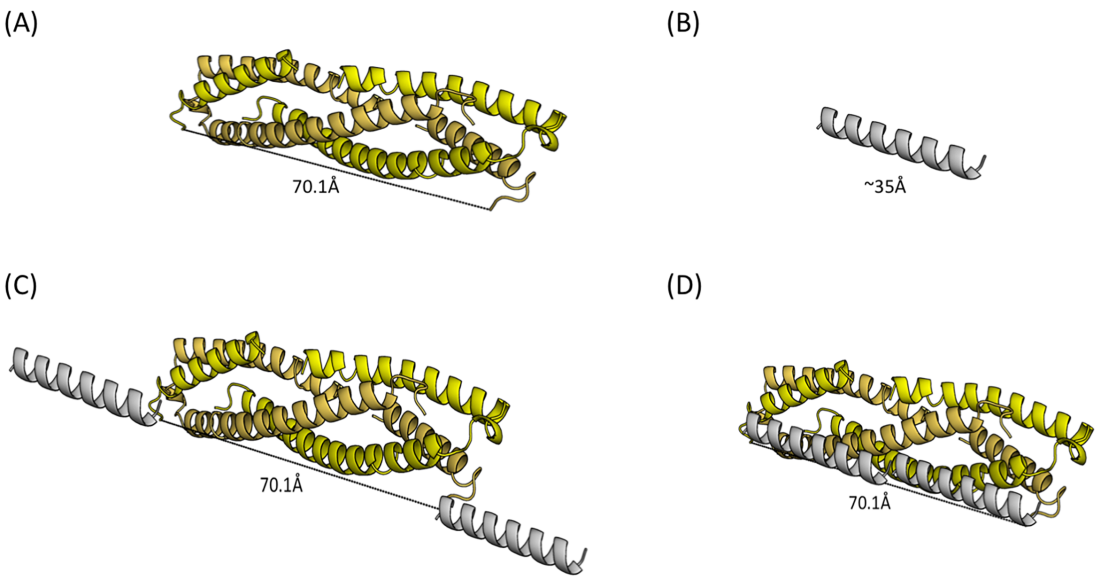

Fig. S9. Self-association and the contribution of the additional C-terminal residues. **(A)** In the MLA10 crystallographic domain-swapped dimer, the C-termini are ~70 Å apart, projecting in opposing directions. The residues 120-144 are predicted to be predominantly helical (see **Fig. S5**). **(B)** When modelled using UCSF Chimera (https://www.cgl.ucsf.edu/chimera/), a helix comprising these residues extends ~35 Å. **(C)** If the helices were to continue without break, they would project away from the body of MLA10 crystallographic domain-swapped dimer. In this situation, they would not support dimer formation in the context of the domain-swap dimer. **(D)** In an event that they folded towards each other as a modelled helix, they would not extend the distance to interact; however, it is plausible that these regions may provide additional contacts that could stabilize further the domain-swap structure.

Reference:

1. Anglister J, *et al.* (1993) Isotope-edited multidimensional NMR of calcineurin B in the presence of the non-deuterated detergent CHAPS. *J Biomol NMR* 3(1):121-126.
2. Cavanagh J, *et al.* (2007) *Protein NMR Spectroscopy: Principles and Practice* (Elsevier) 2nd Ed pp 912-912.
3. Fischer H, *et al.* (2004) Average protein density is a molecular-weight-dependent function. *Prot Sci* 13:2825-2828.
4. Mobli M, *et al.* (2010) A non-uniformly sampled 4D HCC(CO)NH-TOCSY experiment processed using maximum entropy for rapid protein sidechain assignment. *J Magn Reson* 204:160-164.
5. Mobli M, *et al.* (2007) An automated tool for maximum entropy reconstruction of biomolecular NMR spectra. *Nat Methods* 4:467-468.
6. Vranken WF, *et al.* (2005) The CCPN data model for NMR spectroscopy: development of a software pipeline. *Proteins* 59:687-696.
7. Guntert P (2004) Automated NMR structure calculation with CYANA. *Methods Mol Biol* 278:353-378.
8. Cornilescu G, *et al.* (1999) Protein backbone angle restraints from searching a database for chemical shift and sequence homology. *J Biomol NMR* 13:289-302.
9. Maekawa T, *et al.* (2011) Coiled-coil domain-dependent homodimerization of intracellular barley immune receptors defines a minimal functional module for triggering cell death. *Cell Host Microbe* 9(3):187-199.
10. Wen J, *et al.* (1996) Size-Exclusion Chromatography with on-line light-scattering, absorbance, and refractive index detectors for studying proteins and their interactions. *Anal Biochem* 240(2):155-166.
11. Petoukhov MV, *et al.* (2012) New developments in the ATSAS program package for small-angle scattering data analysis. *J Appl Cryst* 45(2):342-350.
12. Rambo RP & Tainer JA (2013) Accurate assessment of mass, models and resolution by small-angle scattering. *Nature* 496(7446):477-481.
13. Schneidman-Duhovny D, *et al.* (2010) FoXS: a web server for rapid computation and fitting of SAXS profiles. *Nucleic Acids Res* 38:W540-544.
14. Fiser A, *et al.* (2000) Modeling of loops in protein structures. *Prot Sci* 9(9):1753-1773.
15. Kabsch W (2010) XDS. *Acta Crystallogr D Biol Crystallogr* 66(Pt 2):125-132.
16. Winn MD, *et al.* (2011) Overview of the CCP4 suite and current developments. *Acta Crystallogr D Biol Crystallogr* 67(Pt 4):235-242.
17. Hao W, *et al.* (2013) Structural basis for the interaction between the potato virus X resistance protein (Rx) and its cofactor Ran GTPase-activating protein 2 (RanGAP2). *J Biol Chem* 288(50):35868-35876.
18. Pannu NS, *et al.* (2011) Recent advances in the CRANK software suite for experimental phasing. *Acta Crystallogr D Biol Crystallogr* 67(Pt 4):331-337.
19. Emsley P, *et al.* (2010) Features and development of Coot. *Acta Crystallogr D Biol Crystallogr* 66(Pt 4):486-501.
20. Bricogne G, *et al.* (2016) *BUSTER version 2.10.2* (Global Phasing Ltd., Cambridge, UK).
21. Croll TI & Andersen GR (2016) Re-evaluation of low-resolution crystal structures via interactive molecular-dynamics flexible fitting (iMDFF): a case study in complement C4. *Acta Crystallogr D Biol Crystallogr* 72(9):1006-1016.
22. Afonine PV, *et al.* (2012) Towards automated crystallographic structure refinement with phenix.refine. *Acta Crystallogr D Biol Crystallogr* 68(Pt 4):352-367.
23. Cesari S, *et al.* (2016) Cytosolic activation of cell death and stem rust resistance by cereal MLA-family CC–NLR proteins. *Proc Natl Acad Sci U S A* 113(36):10204-10209

24. Herrmann T, *et al.* (2002) Protein NMR structure determination with automated NOE assignment using the new software CANDID and the torsion angle dynamics algorithm DYANA. *J Mol Biol* 319:209-227.
25. Evans PR & Murshudov GN (2013) How good are my data and what is the resolution? *Acta Crystallogr D Bio Crystallogr* 69(Pt 7):1204-1214.
26. Chen VB, *et al.* (2010) MolProbity: all-atom structure validation for macromolecular crystallography. *Acta Crystallogr D Bio Crystallogr* 66(Pt 1):12-21.
27. Buchan DWA, *et al.* (2013) Scalable web services for the PSIPRED Protein Analysis Workbench. *Nucleic Acids Res* 41:W349-357.